AD-A172 513 CAVITY COLLAPSE IN ENERGETIC MATERIALS(U) ARMY BALLISTIC RESEARCH LAB ABERDEEN PROVING GROUND MD R B FREY JUL 86 BRL-TR-2748 1/1

UNCLASSIFIED F/G 19/4 NL

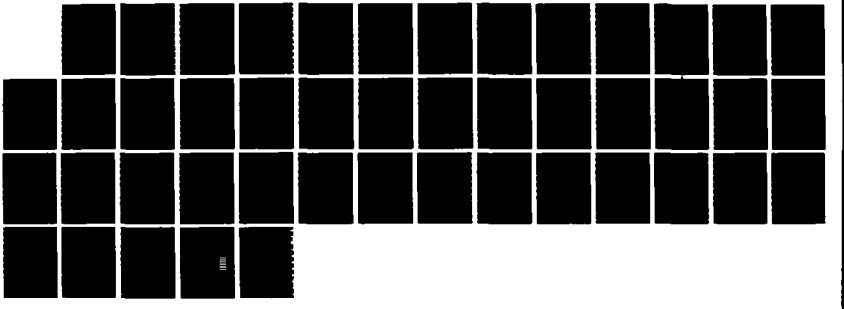

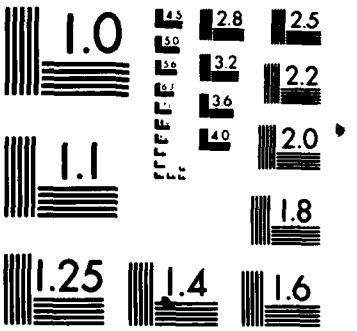

MICROCOPY RESOLUTION TEST CHART
NATIONAL BUREAU OF STANDARDS 1963-A

(12)

AD

US ARMY MATERIEL COMMAND

TECHNICAL REPORT BRL-TR-2748

CAVITY COLLAPSE IN ENERGETIC MATERIALS

Robert B. Frey

July 1986

US ARMY BALLISTIC RESEARCH LABORATORY
ABERDEEN PROVING GROUND, MARYLAND

Destroy this report when it is no longer needed.
Do not return it to the originator.

Additional copies of this report may be obtained from the National Technical Information Service, U. S. Department of Commerce, Springfield, Virginia 22161.

The findings in this report are not to be construed as an official Department of the Army position, unless so designated by other authorized documents.

The use of trade names or manufacturers' names in this report does not constitute indorsement of any commercial product.

UNCLASSIFIED

SECURITY CLASSIFICATION OF THIS PAGE (When Data Entered)

REPORT DOCUMENTATION PAGE		READ INSTRUCTIONS BEFORE COMPLETING FORM
1. REPORT NUMBER Technical Report BRL-TR-2748	2. GOVT ACCESSION NO. AD-A172513	3. RECIPIENT'S CATALOG NUMBER
4. TITLE (and Subtitle) Cavity Collapse In Energetic Materials		5. TYPE OF REPORT & PERIOD COVERED
		6. PERFORMING ORG. REPORT NUMBER
7. AUTHOR(s) Robert B. Frey		8. CONTRACT OR GRANT NUMBER(s)
9. PERFORMING ORGANIZATION NAME AND ADDRESS US Army Ballistic Research Laboratory ATTN: SLCBR-TB Aberdeen Proving Ground, MD 21005-5066		10. PROGRAM ELEMENT, PROJECT, TASK AREA & WORK UNIT NUMBERS 1L162636D221
11. CONTROLLING OFFICE NAME AND ADDRESS US Army Ballistic Research Laboratory ATTN: SLCBR-DD-T Aberdeen Proving Ground, MD 21005-5066		12. REPORT DATE July 1986 13. NUMBER OF PAGES 42
14. MONITORING AGENCY NAME & ADDRESS(if different from Controlling Office)		15. SECURITY CLASS. (of this report) UNCLASSIFIED 15a. DECLASSIFICATION DOWNGRADING SCHEDULE

16. DISTRIBUTION STATEMENT (of this Report)

Distribution Unlimited. Approved for Public Release.

17. DISTRIBUTION STATEMENT (of the abstract entered in Block 20, if different from Report)

18. SUPPLEMENTARY NOTES

19. KEY WORDS (Continue on reverse side if necessary and identify by block number)

Explosive	Initiation
Cavity	Void
Hot Spot	

20. ABSTRACT (Continue on reverse side if necessary and identify by block number)

We have studied the mechanics of cavity collapse in an energetic material. During cavity collapse, several mechanisms can act individually or collectively to produce high temperature hot spots. Our goal is to understand how pressurization rate, cavity size and material parameters affect hot spot formation. For this purpose we have considered the collapse of spherical cavities using a modified form of the model of Carroll and Holt. Using this analysis, we can consider hot spots produced by inviscid plastic work,

DD FORM 1 JAN 73 1473 EDITION OF 1 NOV 65 IS OBSOLETE

UNCLASSIFIED

SECURITY CLASSIFICATION OF THIS PAGE (When Data Entered)

viscoplastic work, gas phase heating, or solid phase compression (which occurs as the result of high pressures produced when material collides at the center of the cavity). Under the proper conditions, each of these mechanisms may be dominant, but viscous heating is the most efficient mechanism and is dominant when the rise time of the pressure is short, viscosity is high, and/or yield stress is low. The conditions under which the other mechanisms are dominant and the dependence of hot spot temperatures on the pressurization rate, cavity size, and material properties are discussed. Cavity size and melt point have an interesting effect on the computed temperatures. Melting is significantly desensitizing when the cavities are small but can be sensitizing for larger cavities.

TABLE OF CONTENTS

LIST OF ILLUSTRATIONS

I. INTRODUCTION

It is well known that cavities, or microporosity, can sensitize an energetic material to shock or compression waves. There are many reasons for this which have been discussed by many authors. Mader[1] in considering shock initiation, proposed a hydrodynamic mechanism in which the upstream surface of a cavity is accelerated by the shock and hits the downstream side of the cavity, producing a high impact pressure which is amplified by convergence effects during the collapse process. In this mechanism, the heating is produced by compression of the solid phase material and plastic or viscoplastic work is not required. Bowden and Yoffe[2] demonstrated that under some conditions gas compression in pores could cause ignition. Other experimental work[3 4] has demonstrated that this is not the controlling mechanism under the usual conditions of shock initiation, but Starkenberg[5] has demonstrated that it can be a dominant mechanism under conditions where the compression rate is relatively low (compared to shock waves) and the cavities are relatively large (a millimeter or more in diameter). Khasainov[6] and Carroll and Holt[7] have discussed heating due to plastic work in the vicinity of collapsing cavities. Carroll and Holt[8] considered inviscid plastic work (in reference 8 they considered viscous effects but did not discuss thermal effects) and Khasainov considered purely viscous (stress varies linearly with strain rate) plastic work. In each case, significant temperature increases were predicted for a thin shell of material around the collapsing cavity. It is also possible that shear bands could form in the vicinity of collapsing cavities. Initiation as the result of shear banding was first discussed by Winter and Field,[10] although not in the context of cavity collapse. The present author discussed shear banding in reference 10 and it appears that shear banding is also a possible ignition mechanism.

A problem with all of the treatments mentioned above is that they do not relate the ignition thresholds to such obvious physical parameters as cavity size and pressurization rate or to such material properties as viscosity, yield strength, and melt point. Much experimental work[11] indicates that particle size (which affects cavity size) has a strong effect on ignition thresholds. Also, it is widely recognized that the pressurization rate must affect ignition thresholds, and this effect has been observed experimentally by Setchell.[12] Of the theoretical treatments mentioned above, only Starkenberg's addresses these two questions, and Starkenberg discusses only the gas compression mechanism. None of the treatments mentioned above discusses the effect of melting.

Our goal in this paper is to combine the various heating mechanisms which can occur in the vicinity of a collapsing cavity into one model and to determine the conditions under which each is dominant. The model, which is described in the next section, is necessarily highly idealized, so we will be interested in general trends rather than specific ignition thresholds. We will consider the effects of pressurization rate, cavity size, viscosity, yield strength, and melt point. Unfortunately, it was not possible to include shear banding in the model, so this mechanism is ignored.

II. PRINCIPAL ASSUMPTIONS USED IN THE MODEL

We based our model on the work of Carroll and Holt[7] and Carroll, Holt, and Butcher.[8] They considered the collapse of a spherical cavity at the center of a spherical shell of solid matrix material. The assumptions of the model are as follows:

1. The flow is spherically symmetric in the vicinity of the cavity, and the pressure in the vicinity of the cavity depends only on radius. These are severe restrictions, but there are two cases where they are reasonable assumptions. The first is the case where rate of pressure increase is sufficiently low that there is never any significant pressure gradient across the diameter of the cavity; i.e.,

$$\Delta P = \frac{dP}{dt}\frac{A}{C} \ll P_{max}, \tag{1}$$

where P is the pressure gradient across the cavity, dP/dt is the rate of pressurization, A is the cavity radius, C is the sound speed, and P_{max} is the maximum applied pressure. For a 1000 micron cavity, assuming a sound speed of 2.5 km/sec, this relation is satisfied as long as the pressurization time (P_{max}/(dp/dt)) is greater than one microsecond. It will thus apply to all the situations of interest except those involving shocks with very short rise times. The second case is where the time required for the shock or compression wave to pass over the cavity is very short compared to the cavity collapse time; i.e.,

$$\frac{A}{C} \ll \tau, \tag{2}$$

where τ is the cavity collapse time. Viscous effects, which will be discussed later, typically require that the cavity collapse time be of the order of a microsecond even for small cavities. Hence, this relation holds for cavities as big as 1000 microns.

2. The matrix material is incompressible. The use of this assumption has several ramifications. First, it limits us to cases where the collapse velocity is much less than the sound speed. By calculation, this was true for the results reported here. Second, it means that we cannot explicitly consider the hydrodynamic mechanism since the heating in this mechanism is due to compression of the solid. However, we will be able to determine when the collapse process leads to pressures where the hydrodynamic mechanism might apply. Finally, we are limited to relatively low applied pressures. Ben Reuven and Summerfield[13] analyzed the case of a collapsing cavity in an inviscid fluid without strength. Their results indicate that compressibility begins to affect the computed pressure in the cavity when that pressure reaches about one gigapascual. When strength and viscosity are considered, the importance of compressibility may be less, but we will generally restrict ourselves to applied pressures of less than one GPa. The computed pressure

in the vicinity of the collapsing cavity may exceed this limit, and when it does we must be aware of the possibility of error.

3. The following constitutive relation applies:

$$S_r = 2\mu\dot{e}_r + \frac{2}{3} Y$$

$$S_\theta = 2\mu\dot{e}_\theta - \frac{1}{3} Y, \tag{3}$$

where μ = viscosity, Y = yield strenth, S_r and S_θ are the principle deviator stresses, and $\dot{e}_r$ and $\dot{e}_\theta$ are the principle deviator strain rates. This relation is appropriate for a rigid-plastic material, and it was our intention to limit ourselves to this case. However, in doing the calculations we found it necessary to relax this assumption as described below.

III. COMPUTATIONAL DETAILS

Carroll and Holt considered a hollow sphere with outer radius b, inner radius a, and porosity α, defined as the ratio of the actual volume to the fully compacted volume, where $\alpha = b^3/(b^3-a^3)$. The equation of motion for this system is

$$\frac{\partial \sigma_r}{\partial r} + \frac{2}{r}(\sigma_r - \sigma_\theta) = \rho \ddot{r}, \tag{4}$$

where σ_r and σ_θ are the principle stresses, r is the radius, and dots imply differentiation with respect to time. Following Carroll and Holt, we note that

$$\sigma_r - \sigma_\theta = S_r - S_\theta = \mu\dot{e}_r + y, \tag{5}$$

and apply the boundary conditions,

$$\sigma_r = P_g \text{ at } r = a$$

$$\sigma_r = -P \text{ at } r = b,$$

where P is the applied pressure and P_g is the pressure in the gas filled cavity.

We also note that

$$\dot{e}_r = + \frac{2}{3} \frac{\dot{B}}{r^3},$$

where $B(t) = a_o^3 - a^3 = b_o^3 - b^3$ (6)

$= a_o^3 (\alpha_o - \alpha)/(\alpha_o - 1)$

and a_o, b_o, and α_o are the initial values of a, b, and α. The equation of motion can then be integrated with respect to the radius and the result expressed as the following differential equation for α:

$$P - P_g - \int_a^b \frac{2Y}{r}\, dr - \int_a^b \frac{4\mu}{3}\frac{\dot{B}}{r^4}\, dr$$

$$= F(\ddot{\alpha}, \dot{\alpha}, \alpha) \tag{7}$$

$$F(\ddot{\alpha}, \dot{\alpha}, \alpha) =$$

$$\frac{\rho a_o^2}{3(\alpha_o - 1)^{\frac{2}{3}}}\left[\frac{\dot{\alpha}^2}{6}\left[(\alpha - 1)^{-\frac{4}{3}} - \alpha^{-\frac{4}{3}}\right] - \ddot{\alpha}\left[(\alpha - 1)^{-\frac{1}{3}} - \alpha^{-\frac{1}{3}}\right]\right] \tag{7a}$$

For convenience, we will refer to the third term on the left side of Eq.(7) as the inviscid plastic yield stress, P_{eq}, and the fourth term as the viscous stress, P_v. The rate of plastic work per unit volume at any point in the flow may be computed from the following equation (14):

$$W = \sum_i \int_o^{e_i^f} S_i de_i, \tag{8}$$

where S_i is the principal deviatoric stress, e_i is the principal deviatoric strain, e_i^f is the final value of the deviatoric strain, and ρ is the density. In our case, we divide the total work, W, into a plastic work term, W_p, and a viscoplastic work term, W_v. Using Eq. (5, 6, and 8) yields the results that

$$\dot{W}_p = \frac{2}{3} Y \frac{\dot{B}}{r^3} \tag{9}$$

and $$\dot{W}_v = \frac{2}{3}\frac{\dot{B}^2}{r^6} \tag{10}$$

Eq. (7) was integrated numerically to determine B, $\dot{B}$, r, and α. Simultaneously, we numerically integrated the heat equation for the material about the cavity to determine the local temperature T:

$$\frac{\partial T}{\partial t} = \frac{K}{\rho_c} \left(\frac{\partial^2 T}{\partial r^2} + \frac{2}{r} \frac{\partial T}{\partial r} \right) + \frac{\dot{W}}{\rho c} , \tag{11}$$

where t is time, K is heat conductivity, and C is heat capacity.

The gas in the cavity was treated using an Abel equation of state,

$$P_g (v - nV_c) = nRT \tag{12}$$

where V is the volume of the cavity, V_c is the covolume of the gas, R is the gas constant, n is the number of moles of gas present, and T is temperature. The pressure was assumed to be uniform throughout the gas phase, but the temperature and density could vary as a function of radius. The temperature was obtained from the heat equation, which was simplified by assuming that the source term, the heat generated by pressure-volume work, was constant everywhere in the gas phase. When the temperature was known in each zone, the pressure could be determined from the following equation,

$$P_g = \frac{\sum_i (V_{oi} - n_i V_c) \frac{T_i}{T_o} P_{go}}{4\Pi \frac{a^3}{3} - \sum_i n_i \dot{V}_c} \tag{13}$$

where V_{oi} the initial volume of the ith element, n_i is the moles of gas in the ith element, T_i is the temperature of the ith element, T_o is the initial temperature, P_{go} is the initial pressure, and a is the cavity radius. Knowing P_g and T_i, Eq.(12) was used to compute the volume of each element of the gas phase.

At the gas-solid interface, the inner most layer of solid and the outermost layer of gas were combined in a single zone. Heat inputs and outputs (by heat conduction, by gas phase pressure-volume work, and by solid phase plastic and viscoplastic work) were averaged over the entire zone. This procedure permitted a little heat to be transferred from the gas phase to the solid phase even when the gas phase heat conductivity was set equal to zero.

The computational mesh was set up so that the zones near the gas-solid boundary were always very small. The zone size gradually increased further from the boundary. The thickness of the innermost zone in the solid phase was initially 0.02 times the cavity radius and during the calculation it was never

more than 0.25 times the instantaneous cavity radius. The calculation was rezoned to use a smaller zone size whenever this criterion was violated or when a large temperature difference was noted between the two innermost zones. Because of the small zone size, it was necessary to violate the VonNeumann stability condition in order to achieve reasonable computer times. However, the finite difference calculation was carried out using a predictor/corrector technique with several iterations at each time step, and no problems with stability were observed.

The yield strength, Y, was varied in the calculations to observe its effect on the temperature achieved. When the temperature was more than $30^{\circ}K$ below the melt point, Y was constant, and above the melt point it was zero. In the $30^{\circ}K$ range of temperature just below the melt point, Y decreased linearly as a function of temperature. Two forms of the viscosity, μ, were used. In the constant viscosity model, the viscosity was independent of both temperature and pressure. This was convenient for studying the effect of viscosity, but not very realistic. In the variable viscosity model, the viscosity varied according to the following equation:

$$\mu = 1000 \text{ poise for } T < T_{melt}$$

$$\mu = \mu_o \exp \frac{P}{P_s} \exp \frac{E}{T} - \frac{E}{T_s} \quad \text{for } T > T_{melt}, \tag{14}$$

where P_o, T_s, u_o, and E are constants. This type of relation has been discussed by Frankel[15] and Bridgeman.[16] The value of 1000 poise for the viscosity below the melt point was chosen on the basis of Khasainov's[6] analysis of Wackerle's[17] data for the decay of pressure behind a shock wave in porous PETN. In another paper,[18] Wackerle suggests a higher value of 10,000 poise, and at times we have used this value instead of 1000 poise in equation (14). For u_o, E, and T_s, we used values appropriate to TNT and determined by fit to very limited data in reference 19. For P_o we used a value appropriate to nitrobenzene and determined from data in the International Critical Tables. These values and values for some other parameters are shown in Table 1. In using these parameters, we are not attempting to model any particular material, but we are choosing parameters which we feel are representative of secondary explosives. The melt point was varied, but where it is not specified it is $353^{\circ}K$. Unless stated otherwise, we also assumed in all cases that the melt point increased by 200°/GPa. Gas phase heat conductivities increase greatly with pressure. Starkenberg[8] has shown that this effect must be included if one is to correctly model the ignition of explosives due to gas compression. In the calculations reported here, we restrict ourselves to a constant gas phase heat conductivity, but use a value ten times that of air at atmospheric pressure and room temperature. We also discuss the effect of varying the gas phase heat conductivity.

Table 1. Material Properties Used

u_o = 1.39 x 10-2 kg/m/s

T_s = 358°K

E = 3,880°K

P_s = 0.165 GPa

ρ = 1.6 x 10^3 kg/m^3

C = 1.4 x 10^3 joule/(kg°C)

K = 0.262 joule/(m °C s)

V_c = 28 cm^3/mole

K_g = .33 joule/(m °C s)

C_g = 1 x 10^3 joule/(kg °C)

α_o = 1.05

(K_g and C_g are the gas phase heat conductivity and heat capacity. They were assumed to be constant for simplicity, but see text.)

For simplicity, we had hoped to use a rigid plastic model, as shown by equation (4) for determining the deviator stress. In some situations, however, the cavity "bounces" as it collapses. In these cases, e_r changes sign, and if the rigid plastic model is used the deviator stresses all suddenly change sign. This causes convergence problems in the numerical integration of equation (6). In principle, this problem could be eliminated by using the full elastic-plastic form of the equations, as described in reference 10, but we wished to keep the problem as simple as possible. Consequently, we invented an artificial elastic behavior. During the first phase of the collapse, the matrix is treated as rigid-plastic as described above. If the cavity "bounces" and the radius begins to grow, the plastic yield stress, P_{eq}, is computed from the following equations:

$$P_{eq} = F(\alpha) \int \frac{2Y}{r} dr \tag{15}$$

$$F(\alpha) = 1 - \frac{\alpha - \alpha_{min}}{\alpha' - \alpha_{min}} \text{ for } \alpha < 2\alpha' + \alpha_{min} \tag{16}$$

$$F(\alpha) = -1 \text{ for } \alpha > 2\alpha' + \alpha_{min}$$

(17)

$$\alpha' = \alpha_{min} + \frac{Y}{2G}(\alpha_{min} - 1) \quad ,$$

where α_{min} is the lowest porosity obtained on the preceding cycle of collapse and G is the shear modulus. If the cavity has been expanding and begins to contract, P_{eq} is given by equation (15) with $F(\alpha)$ defined as follows:

$$F(\alpha) = \frac{\alpha_{max} - \alpha}{\alpha_{max} - \alpha'} - 1 \qquad \alpha > 2\alpha' - \alpha_{max} \tag{18}$$

$$F(\alpha) = 1 \qquad \alpha < 2\alpha' - \alpha_{max} \tag{19}$$

$$\alpha' = \frac{(2G\,\alpha_{max} + Y)}{2G + Y} \quad ,$$

where α_{max} is the largest porosity obtained on the last cycle of expansion. P_{eq}, calculated for equation (15) to (17), replaces the third term on the left side, of equation (7).

IV. PRESSURE AMPLIFICATION

During cavity collapse, the material in the vicinity of the cavity may be accelerated to relatively high velocity. In the final stage of cavity collapse this material must be abruptly decelerated, and the pressure may obtain very high values, many times that of the applied pressure. This is called pressure amplification or overshoot. In an inviscid, strengthless fluid overshoot always occurs (for instance, see reference 13). When overshoot occurs, the hydrodynamic ignition mechanism, which involves compression of the solid matrix material, may be possible. When overshoot does not occur, the hydrodynamic mechanism will not be important (at least for the relatively low applied pressures which are considered here).

When the effects of viscosity and strength are considered, overshoot is not inevitable. It is important to understand when it does and does not occur. If the strength is sufficiently high and the pressurization rate is sufficiently low, the inviscid plastic yield stress (P_{eq}, the third term on the left side of equation 7) will increase (as the cavity collapses) fast enough to keep up with the applied pressure, and high collapse velocities do not occur. A dimensionless parameter, N_1, which describes this effect is the following:

$$N_1 = \frac{A}{Y}\frac{DP}{dt}\sqrt{\frac{\rho}{Y}} \tag{20}$$

where A is initial cavity radius, P is pressure, t is time, ρ is density, and Y is the inviscid yield strength. Figure 1 shows the result of two calculations where the applied pressure was 0.4 GPa, the pressurization time was 10 microseconds, the viscosity was very low (1 poise), and the yield strength, Y, was 0.07 GPa. With a cavity size of 100 microns, the plastic yield stress keeps up with the imposed pressure and the cavity undergoes a "gentle" collapse. For larger cavities, with other parameters the same, P exceeds P_{eq} by a large amount early in the collapse process, and the radial velocity becomes large. When the cavity collapse is nearly complete, P_{eq} overshoots P, and the cavity "bounces". P_{eq} can become very large in this case, producing pressures which invalidate this model but make Mader's hydrodynamic model possible. Based on our calculations, the critical value of N_1 is about 1.0.

Viscous effects can,also prevent overshoot. Khasainov, in discussing purely viscous flow (Y=0) and infinitesimal pressure rise times, introduced another nondimensional parameter, which determines whether viscous damping can absorb the available energy fast enough to prevent the cavity from "bouncing." This parameter, N_2, is defined by the following expression:

$$N_2 = \frac{A\sqrt{\rho P}}{\mu} . \qquad (21)$$

Figure 2 shows the results of two calculations which have a short risetime (1 microsecond), a yield strength of 0.035 GPa, an initial cavity size of 100 microns, and viscosities of 200 and 1000 poise. N_1 is large (2.73) so it permits the possibility of large collapse velocities and pressure overshoot in all cases. With the smaller viscosity, the cavity bounces and pressure overshoot occurs; with the higher viscosity, the cavity collapses "gently." Based on our calculations, the critical value of N_2 is about one.

If both N_1 and N_2 are greater than one, pressure overshoot can occur and hydrodynamic heating is possible. Figures 3 and 4 are intended to provide some perspective on the range of cavity sizes, pressures, and pressurization rates for which this can happen. In Figure 3, we have plotted the pressurization rate versus the cavity size on the curve $N_1 = 1$ for the case where $\rho = 1.6$ g/cm^3 and Y = 0.035 GPa. In Figure 4, we have plotted the cavity radius as a function of pressure on the curve $N_2 = 1$. If either N_1 or N_2 is less than one, pressure overshoot does not occur and the hydrodynamic mechanism is not possible. If both are greater than one, hydrodynamic heating may occur as well as viscous and plastic work. Under shock wave conditions, where pressurization rates are very high, Figure 3 indicates that overshoot is possible, based on the N_1 criterion and the parameters mentioned above, for cavities larger than about one micron. However, if the pressurization rate was reduced to 0.052 GPa/microsecond, which is slow when compared to shock waves but still large when compared to many stimuli, a cavity as large as 1000 microns could collapse without overshoot. Figure 4 shows that for an applied pressure of 0.4 GPa, the N_2 criterion prevents overshoot for cavities as large

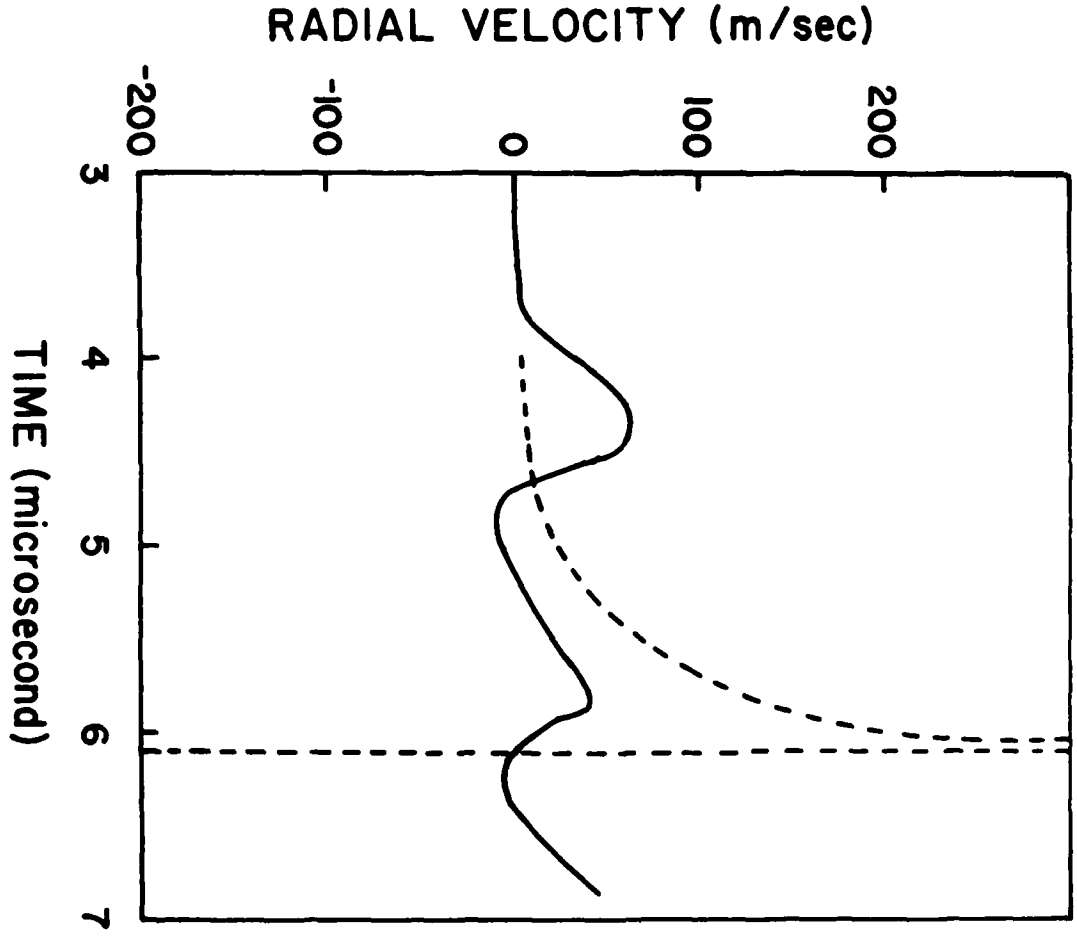

Figure 1a. The radial velocity of two collapsing cavities is shown as a function of time. τ = 10 microseconds; Y = 0.07 GPa, and μ = 1.0 poise. For the solid curve, A = 100 microns; for the dashed curve, A = 400 microns.

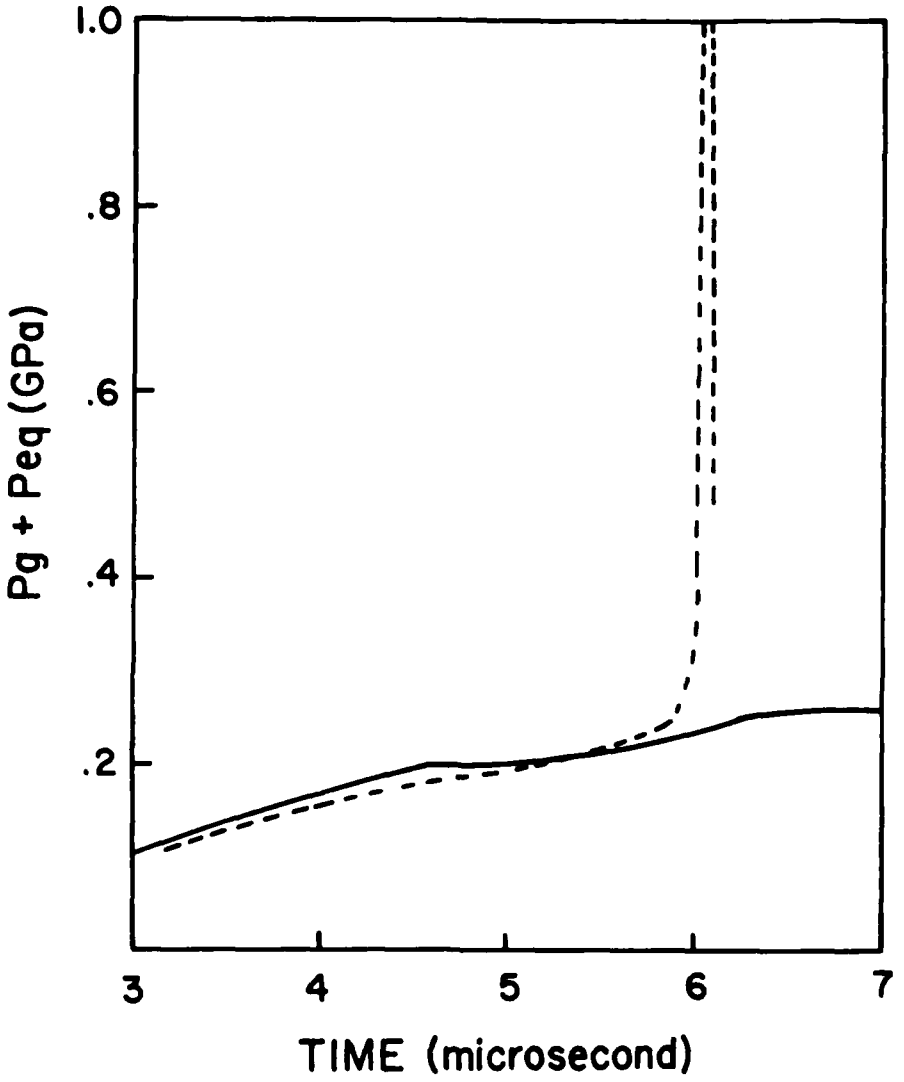

Figure 1b. $P_g + P_{eq}$ is shown as a function of time for the same two calculations show in Figure 1a.

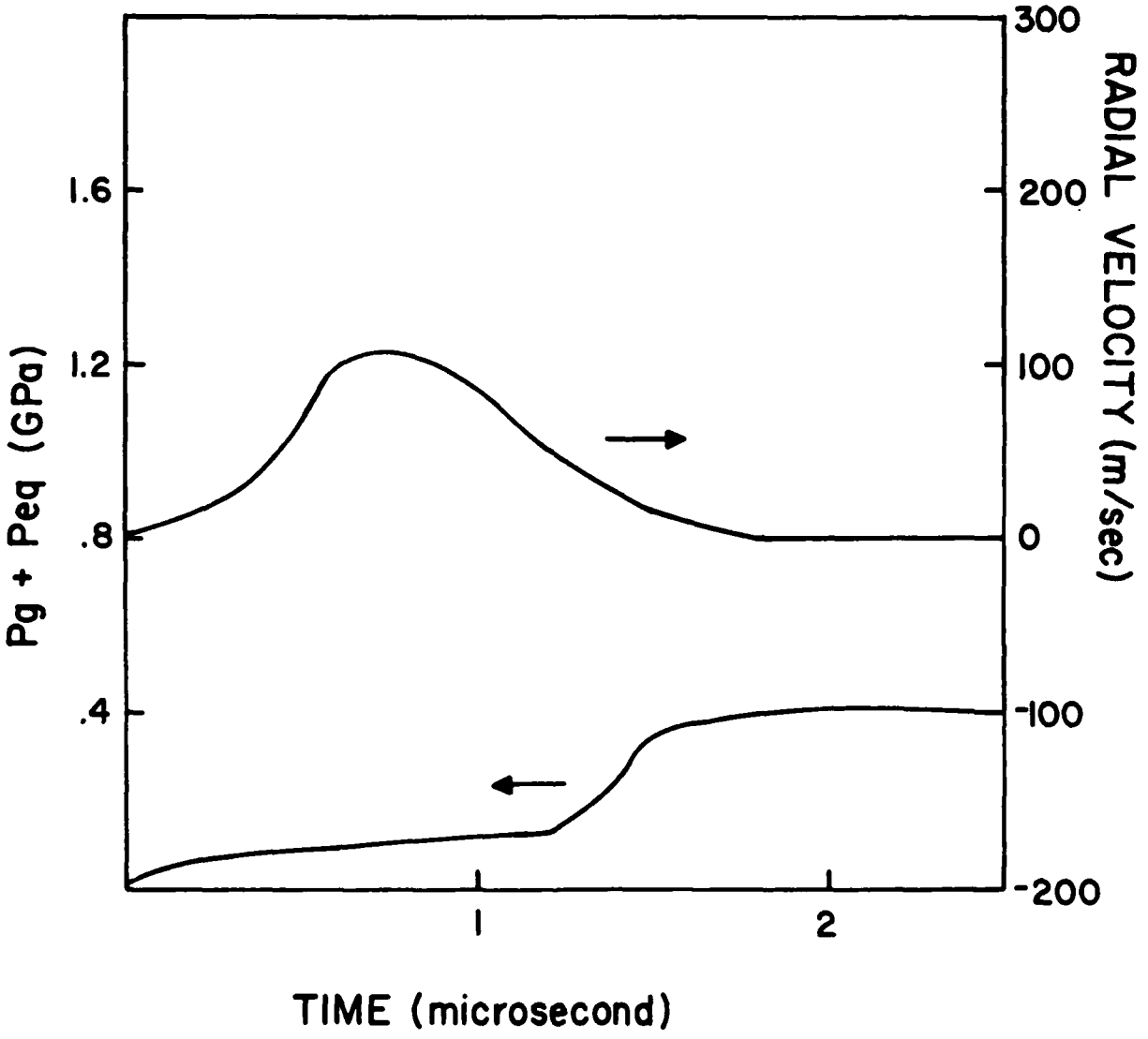

Figure 2a. $p_g + P_{eq}$ and radial velocity are shown as functions of time for a calculation with A = 100 microns, Y = 0.035 GPa, τ = 1 microsecond, and μ = 1000 poise.

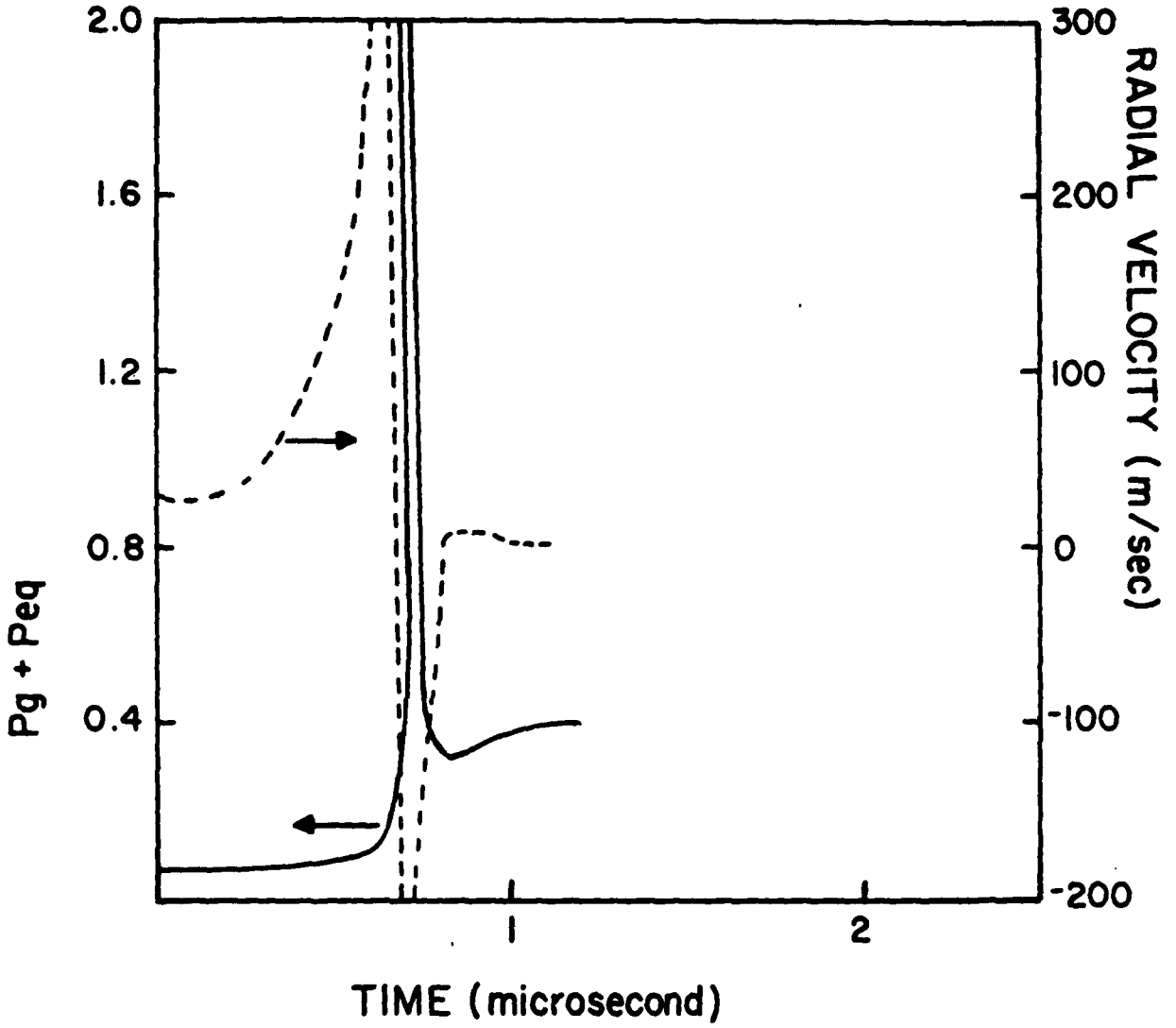

Figure 2b. $P_g + P_{eq}$ and radial velocity are shown as functions of time for a calculation identical to Figure 2a, except μ = 200 poise.

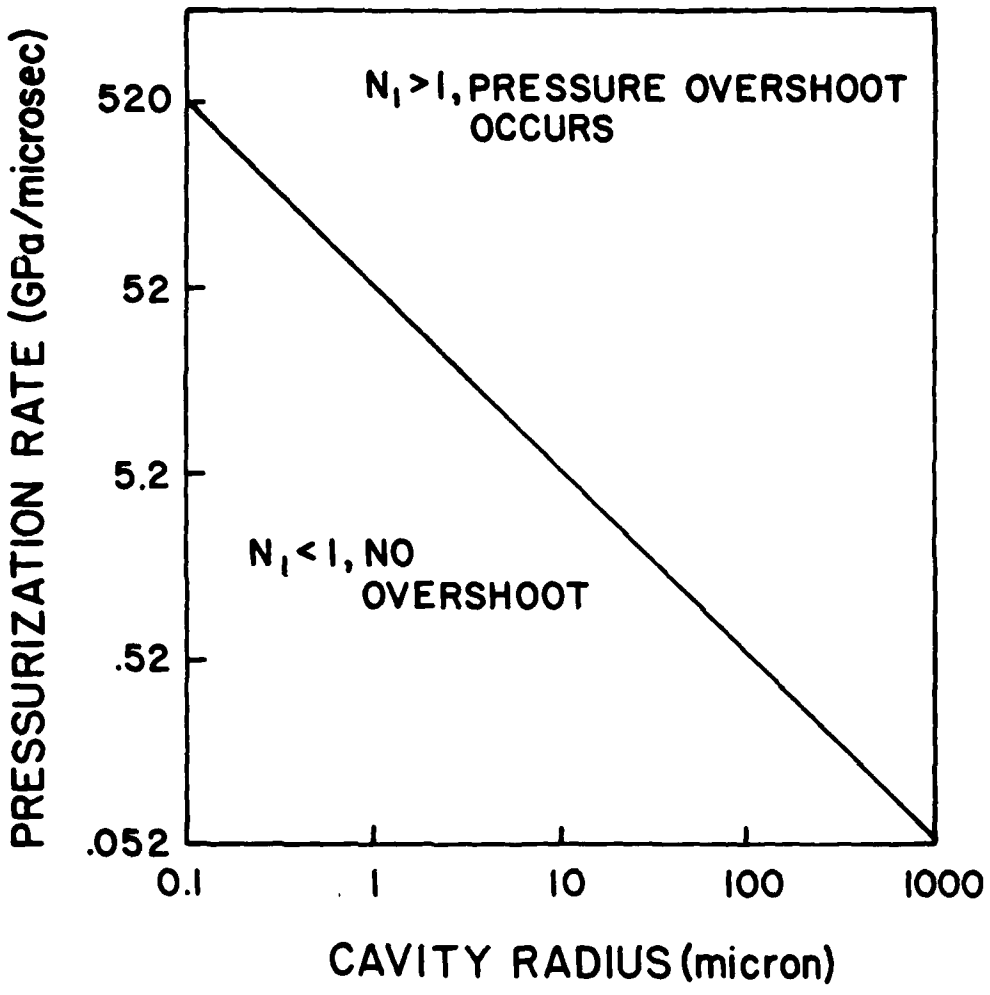

Figure 3. The Curve $N_1 = 1$ is plotted for the case where Y = 0.035 GPa and $\rho = 1.6$.

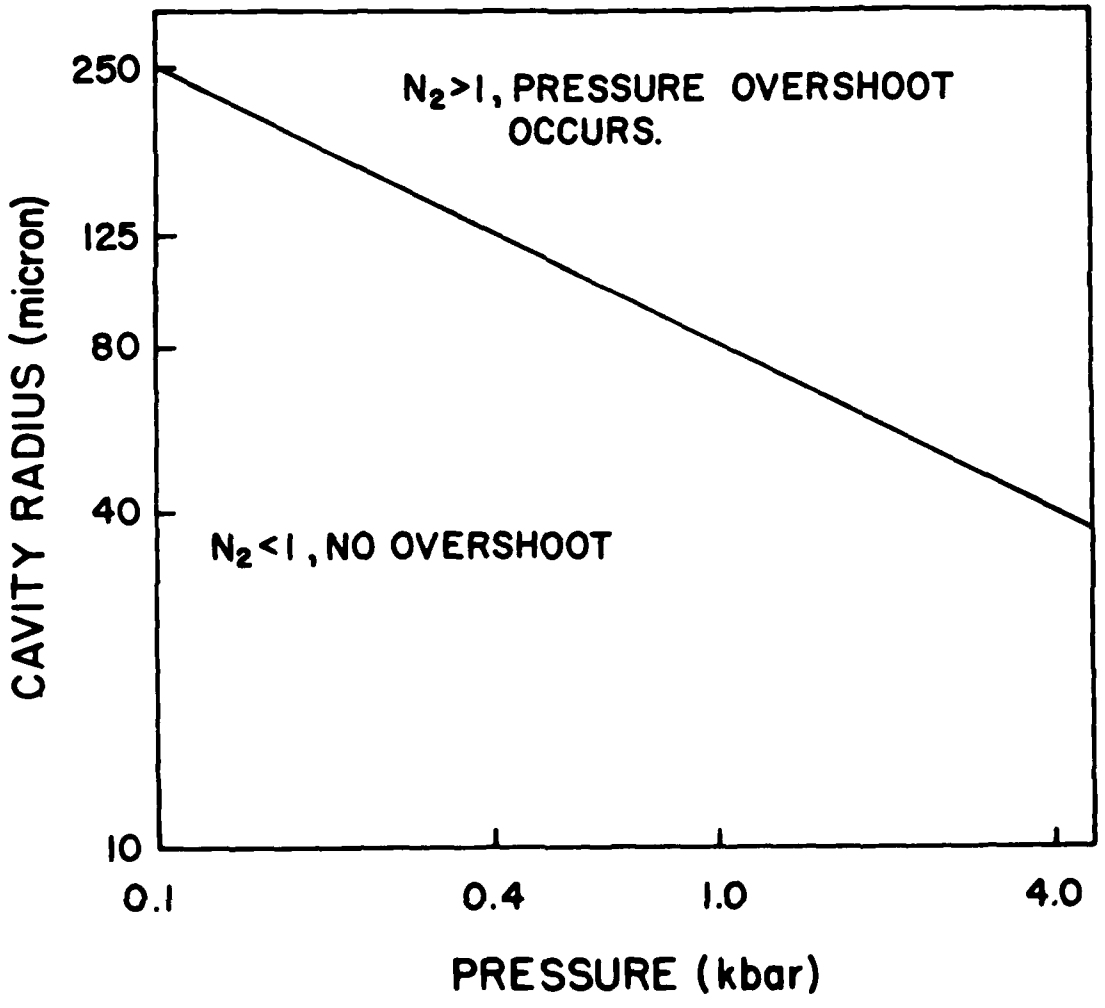

Figure 4. The curve $N_2 = 1$ is plotted for the case where $\mu = 1000$ poise and $\rho = 1.6$.

as 40 micron. Figure 4 was computed with a viscosity of 1000 poise. If this value was raised to 10,000 poise, as suggested by Wackerle[18] the cavity size required for overshoot would increase by an order of magnitude.

V. VISCOPLASTIC HEATING

We will now consider the heating which occurs in the vicinity of the collapsing cavity due to viscoplastic work. The temperature which is produced is controlled by a number of factors, which are described as follows:

1. The relation between the cavity collapse time and the pressurization time. The energy dissipated in the vicinity of the cavity is the integral of the pressure with respect to the change in volume. If the pressurization time is large compared to the collapse time, most of the volume change occurs while the pressure is low, and the energy dissipated is relatively small (but not negligible). Two characteristic collapse times may be considered. One is an inertial collapse time, t_i, which applies to inviscid flows and is given by the following expression [13]:

$$t_i = A \left(\frac{\rho}{P}\right)^{\frac{1}{2}} \tag{22}$$

For large cavities (greater than a millimeter) it is frequently the controlling parameter. The second is a viscous collapse time, t_v, which is independent of cavity size (a surprising fact in the opinion of this author). Khasainov[6] gave the following expression for t_v:

$$T_v = \frac{4\mu}{P} . \tag{23}$$

For a viscosity of 1000 poise and an applied pressure of 0.4 GPa, t_v is about one microsecond. Since it is independent of cavity size, it is frequently the controlling parameter for small cavities (less than a millimeter). Figure 5 shows how the dissipated energy varies with the rise time, τ, of the pressure for a calculation with a cavity size of 40 micron, a pressure of 0.4 GPa, a yield strength of 0.07 GPa, and a viscosity of 1000 poise. The curve is "S" shaped with high dissipated energy for short rise times and low dissipated energy for long rise times. For the situation in Figure 5, the ratio of t_v/τ is the important parameter, and the dissipated energy changes as this parameter changes from more than one to less than one.

This has obvious implications for initiation by a ramped pressure wave. If $\tau > t_v$, hot spot formation will be much more difficult. As mentioned above, for μ = 1000 poise and P = 4 kbar, t_v is about 1 microsecond. At 30 kbar, t_v drops to about 0.13 microseconds. In situations of interest to explosive initiation, even very short rise times can be significantly desensitizing.

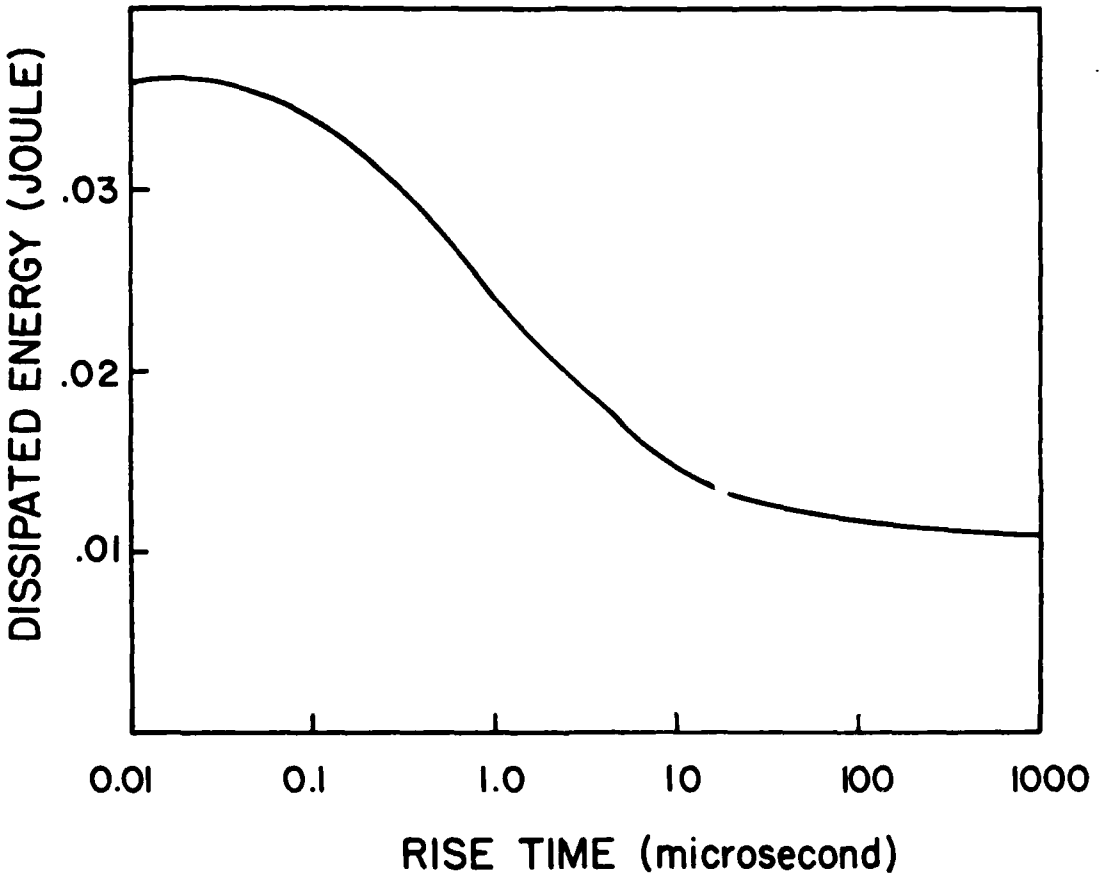

Figure 5. Energy dissipated at a cavity is shown as a function of rise time for a calculation with P = 0.4 GPa, A = 40 micron, Y = 0.07 GPa, and μ = 1000 poise.

2. The relation between inviscid plastic work and viscoplastic work. Depending upon circumstances, the plastic work may be predominantly of the inviscid type (controlled by the yield strength Y) or the viscous type (controlled by viscosity). From equations 9 and 10, we can see that viscoplastic work has a much stronger dependence on radius than does inviscid plastic work. Therefore, when viscoplastic work dominates, we expect the dissipation to be more localized and the temperature to be higher. Futhermore, the inviscid plastic yield stress goes to zero at the melt point, and this limits the heating which can be caused by inviscid plastic work. We find that there is a critical parameter, N_3, which determines whether viscous or inviscid effects dominant. It is the quotient of N_1 divided by N_2 and is expressed as follows:

$$N_3 = \frac{\mu\sqrt{\frac{P}{Y}}}{Y\tau} \quad , \tag{24}$$

where μ is viscosity, P is the applied pressure, Y is the inviscid yield strength and τ is the rise time of the applied pressure. When N_3 is much greater than one (high viscosity, low yield strength, low rise time) viscous effects dominate. Figure 6 illustrates the effect of N_3. It is a plot of the maximum temperature, T, obtained in the solid phase in the vicinity of a collapsing cavity, as a function of the rise time of the applied pressure for calculations where the viscosity was 1000 poise, the initial cavity radius was 40 microns, the applied pressure was 0.4 GPa, and the yield strength was 0.07 GPa. The curve has an "S" shape, and the transition from low to high temperature occurs when N_3 is about one. For the situation in Figure 6, the parameter t_v/τ changes from less than one to greater than one at about the same place, and this increases the effect of rise time on the temperature. As can be seen, the computed temperature is very strongly dependent on rise time, with the transition from low to high temperatures occurring for rise times in the one to ten microsecond range. Figure 7 shows the effect of viscosity on the maximum computed temperature (solid phase). The cavity size was 40 microns; the applied pressure was 0.4 GPa, and two curves are shown with different pressurization times. The temperatures increase with increasing viscosity, and the most rapid increase occurs as N_3 changes from less than one to more than one. Figure 8 shows how the rise time varies with the applied pressure P on the curve N_3 = 1 when μ = 1000 poise and Y = 0.035 GPa. For shock waves, where is very short, viscous heating will be dominant, and high temperatures are expected. With slower pressurization rates, plastic work may be dominant, and the temperature will be lower.

3. Cavity size and level of applied pressure. The maximum energy available for dissipation at the cavity is the product of the cavity size and applied pressure. These parameters also influence the computed temperatures by their effect on the parameters N_1, N_2, and N_3 discussed above. It is interesting to note that in a purely hydrodynamic model, with plastic work and

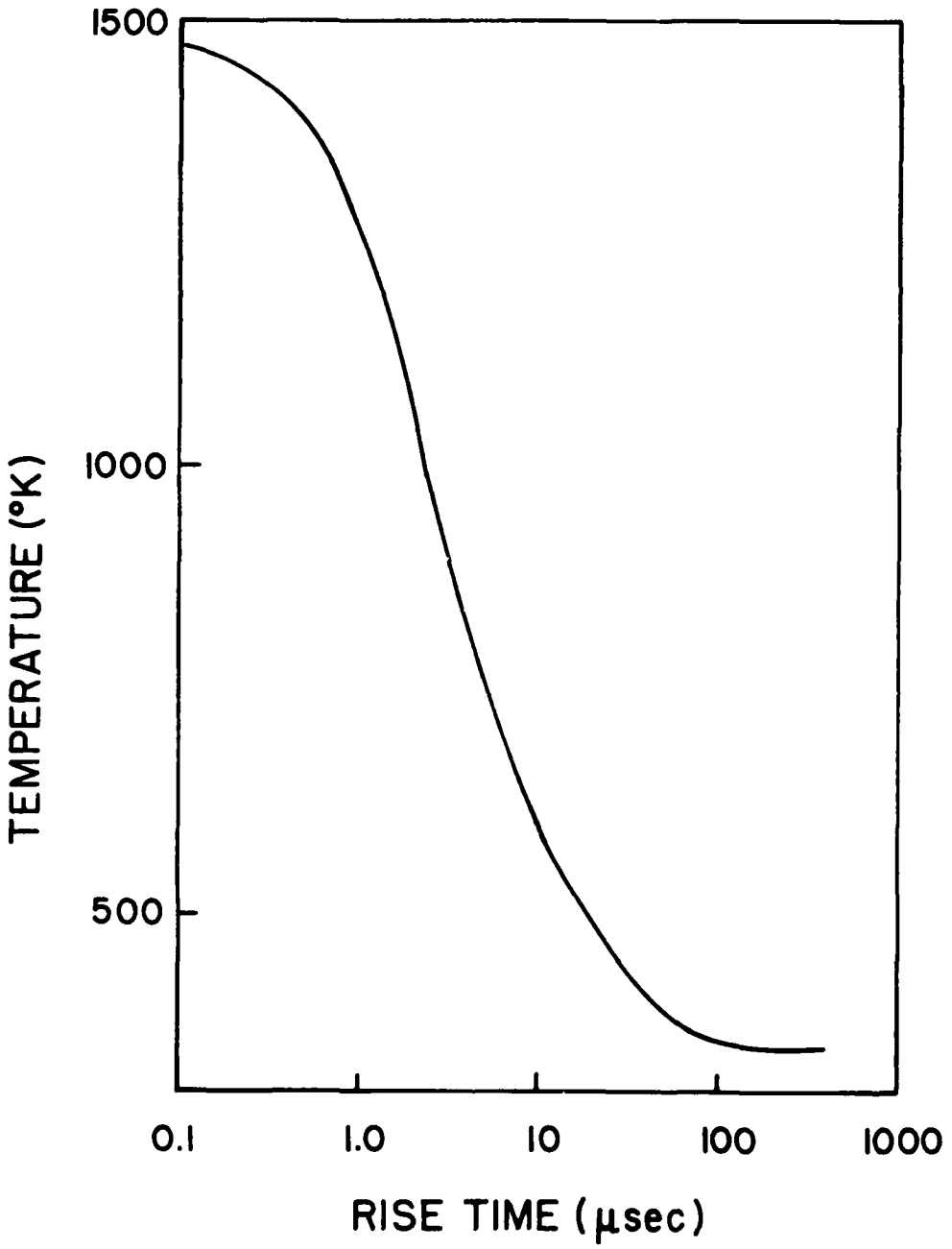

Figure 6. The maximum temperature is plotted as a function of the rise time for a case where P = 0.4 GPa, A = 40 microns, Y = 0.07 GPa, and μ = 1000 poise.

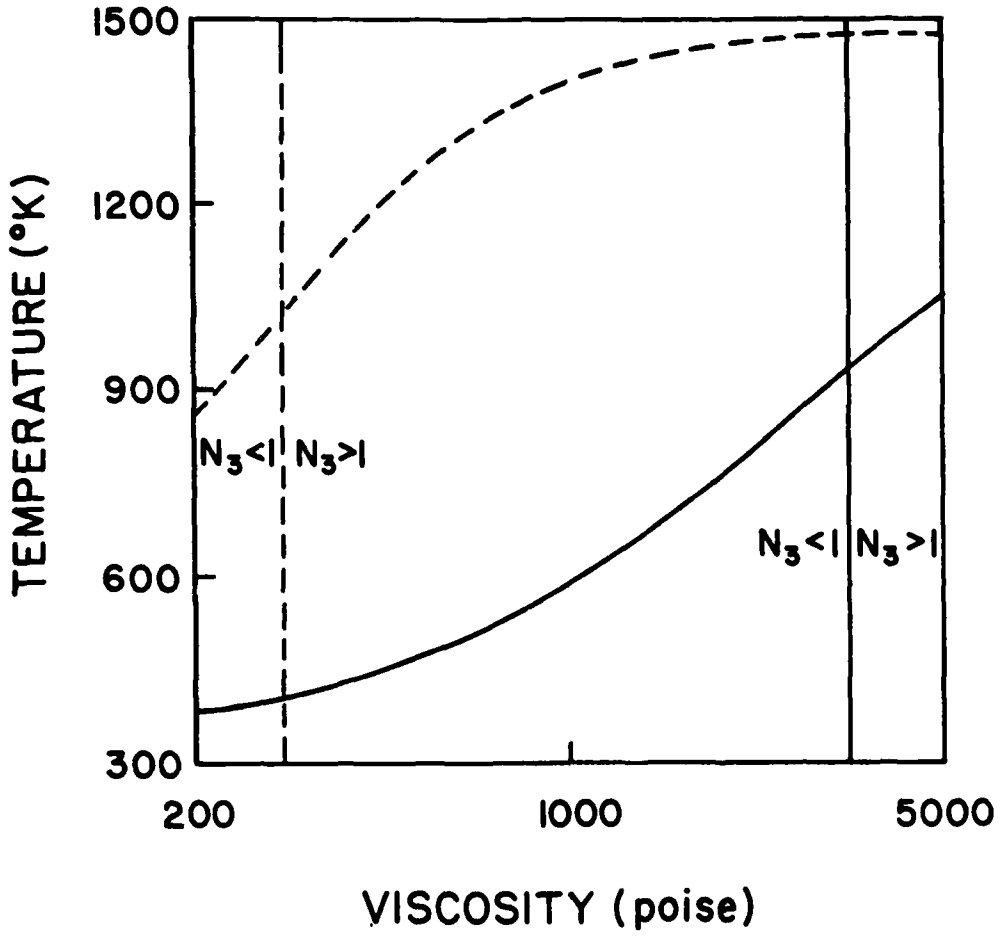

Figure 7. Temperature is plotted as a function of viscosity for two calculations with A = 40 micron, Y = 0.07 GPa, and P = 0.4 GPa. For dotted curve τ = 1 microseconds; for the solid curve τ = 10 microseconds.

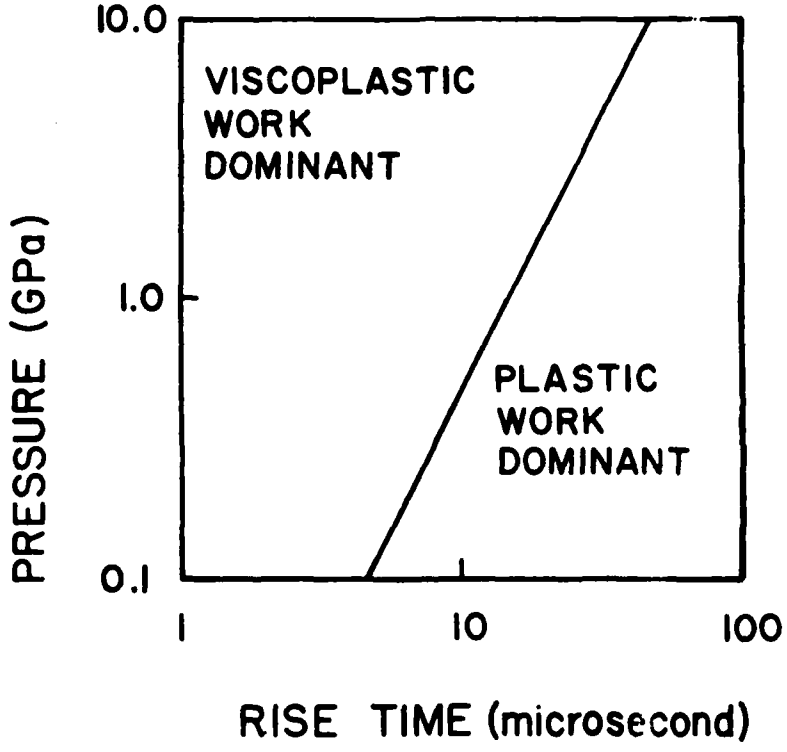

Figure 8. The Curve N_3 = 1 is plotted for the case where Y = 0.035 GPa and μ = 1000 poise.

gas phase heating ignored, the temperature which can be achieved at a cavity is independent of cavity size if the rise time is infinitesimal (the size of the hot spot increases with cavity size, but its temperature does not). However, when plastic work is considered, cavity size has a strong effect on the results. This is shown in Figure 9. The upper curve in Figure 9 shows how the maximum computed temperature (in the solid phase) varies as a function of cavity size for a series of calculations with τ = 1000 poise, τ = 0.1 microseconds, and Y = 0.07 GPa. For this series of calculations, N_3 is large, and viscous heating dominates. Rather high temperatures are thus computed over the entire range of cavity sizes, but the temperature increases with cavity size. When the cavity size exceeds 100 micron, N_2 becomes larger than one, and pressure overshoot occurs. A sharp increase in the temperature occurs because the cavity radius is driven down to a very small value, and this causes greater localization of the energy (the high pressure may also cause hydrodynamic heating, but we do not consider that effect here). The lower curve in Figure 9 shows similar results for calculations with τ equal to ten microseconds. In this case, N_3 is less than one, and the temperatures are relatively low until the cavity size reaches 400 microns. At that point, both N_1 and N_2 become greater than one; overshoot occurs, and high temperatures are achieved.

4. Heat conductivity. Khasainov[6] noted that heat conductivity did not significantly effect the temperature achieved unless the cavity size was less than one micron. He noted that the characteristic time for the cooling of the surface of a sphere is

$$t_c = A^2 \rho C/K, \tag{25}$$

where A is cavity radius, ρ is density, C is heat capacity, and K is heat conductivity. For a one micron cavity, t_c is of the order of ten microseconds, and for bigger cavities it increases rapidly. We have already seen that t_v is of the order of one microsecond when the pressure is 0.4 GPa and the viscosity is 1000 poise. Thus cavity collapse should be complete before heat conduction can significantly affect the results. In the calculations which we have performed, with cavities in the range of 1 to 1000 microns, we have seen no effect due to heat conductivity unless gas compression was a major contributing mechanism (this will be discussed in the next section).

5. The effect of yield strength and initial gas pressure. Yield strength (Y) and the initial gas pressure, P_{go}, in the cavity affect the results in a way that may seem surprising. Although there are exceptions, high strength generally reduces the temperature, sometimes markedly so. The results of some calculations demonstrating this are shown in Table II. The effect of high strength is to shift the dissipation from viscous to plastic forces and to increase the final radius of the cavity. Both of these effects are desensitizing. Higher values for the initial gas pressure are desensitizing for the same reason. The effect of initial gas pressure in two pairs of calculations is shown in Table III. The calculations on the last two lines of Table III are cases where gas phase heating contributed significantly to the result, but even here a lower gas initial pressure produced a higher temperature.

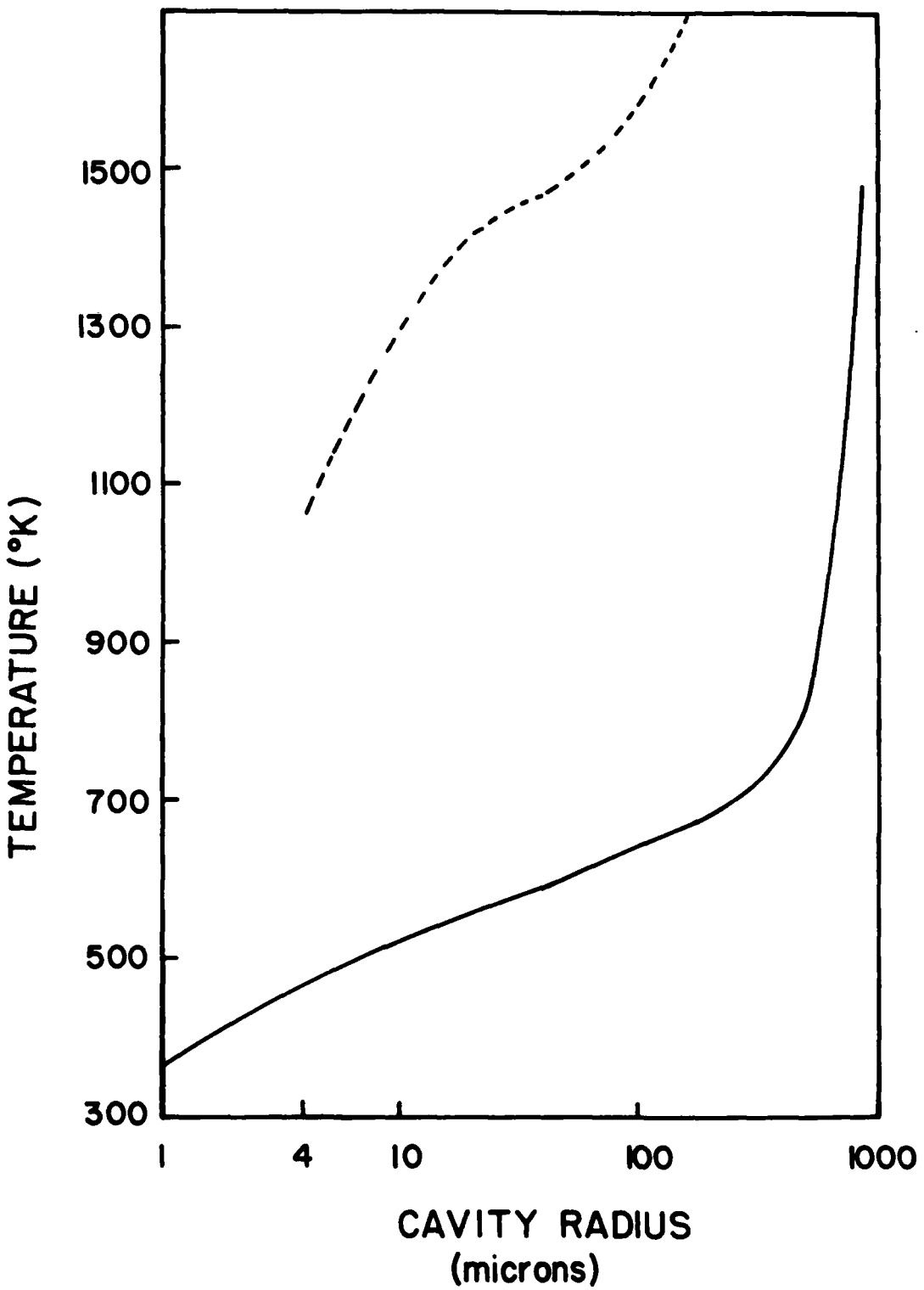

Figure 9. The maximum temperature is plotted as a function of the cavity radius for two cases where P = 0.4 GPa, μ = 1000 poise, and Y = 0.07 GPa. For the dotted curve τ = 0.1 microsecond; for the solid curve τ = 10 microsecond.

TABLE II: EFFECT OF STRENGTH ON COMPUTED TEMPERATURE.

The applied pressure is 0.4 GPa and the viscosity is 1000 poise.

Cavity Size (microns)	Rise Time (microseconds)	Yield Strength (GPa)	Gas Phase Heat Conductivity $\frac{\text{joule}}{\text{m}^\circ\text{C}}$	Computed Temperature ($^\circ$K)
400	10	0.07	0	749
400	10	0.007	0	976
1000	100	0.07	0	360
1000	100	0.007	0	687
1000	100	0.07	33×10^3	484
1000	100	0.007	33×10^3	898

6. The effect of melt point and the temperature dependence of viscosity. The calculations shown so far all used the constant viscosity model and a melt point of 353°K. Varying the melt point and using the variable viscosity model (equation 14) have some interesting effects on the results. When the constant viscosity model is used and $N_3 << 1$, inviscid plastic work dominates, and the temperature is limited to the melt point. With the constant velocity model and $N_3 >> 1$, viscous effects dominate, and the temperature is not affected much by melt point. A better understanding of the real effect of melting is probably provided by the variable viscosity model which allows for a reduction of viscosity as well as yield strength upon melting. Figure 10 shows a comparison of the maximum temperature computed with the variable and constant viscosity models. The temperature is plotted as a function of cavity radius for a case where P = 0.4 GPa, τ = 0.1 microsecond, and Y = 0.07 GPa. With the constant viscosity model, $N_3 >> 1$, viscous effects are dominant, and the temperature is relatively high for all radii. When the variable viscosity model is used, the computed temperatures are much lower (approaching the melt point) for small cavities, but they are quite large for big cavities and may even exceed those computed with the constant viscosity model. With the variable viscosity model, melting

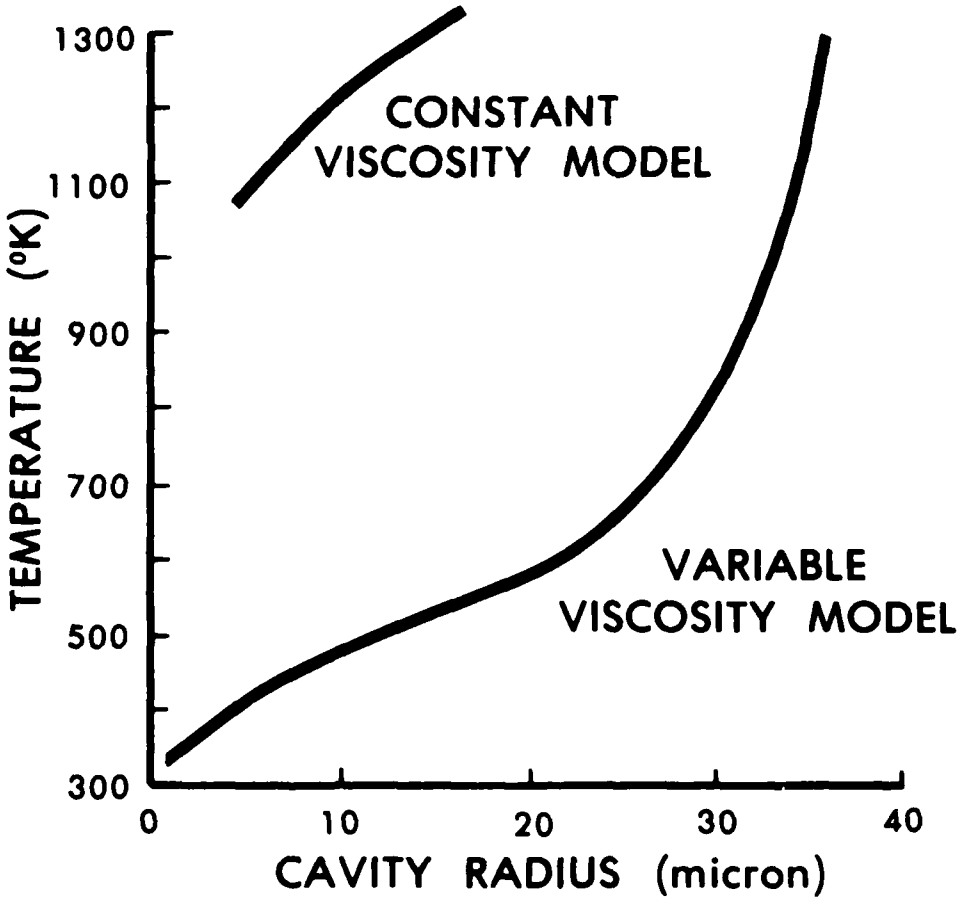

Figure 10. The maximum temeprature, computed as a function of cavity radius, is shown for the constant and variable viscosity models. P = 0.4, τ = 0.1 microsecond, and Y = 0.07 GPa.

TABLE III. EFFECT OF INITIAL GAS PRESSURE.

The applied pressure is 0.4 GPa, the viscosity if 1000 poise, and the yield strength is 0.07 GPa.

Cavity Radius (microns)	Rise Time (microseconds)	Gas Phase Heat Conductivity $\frac{\text{joule}}{\text{m}^\circ\text{C sec}}$	Initial Gas Pressure (atm)	Maximum Temperature ($^\circ$K)
400	10	0	0.0001	1773
400	10	0	1.0	749
1000	100	33×10^3	0.01	635
1000	100	33×10^3	1.0	484

reduces the viscosity and reduces the heating as long as the pressure in the vicinity of the cavity (where the deformation is concentrated) is low. However, in the final stage of cavity collapse, the pressure may rise, and this will increase the viscosity and the rate of heating. For small cavities, where pressure amplification does not occur, melting tends to be strongly desensitizing when the variable viscosity model is used. With large cavities, melting may make overshoot more likely, by reducing viscosity (and thus increasing N_2). In this case the variable viscosity model may give higher temperatures than does the constant viscosity model. However, the most important observation is that melting can be strongly desensitizing for small cavities (of the order of 4 microns or less).

VI. GAS PHASE HEATING

With the exception of the last two lines of Tables II and III, gas phase heating contributed a negligible amount to all of the calculations discussed so far. This was demonstrated by running the calculations with the gas phase heat conductivity set equal to zero as well as to the value specified in Table I. However, in some cases, the gas phase heating can have a significant or dominant effect. The conditions under which gas phase heating is dominant are relatively large cavity size (so the gas will contain enough heat energy to affect the solid significantly), long rise time or low viscosity (otherwise viscous effects dominate), and a melt point below the ignition temperature (to suppress inviscid plastic work effects). When all of these conditions are met, gas phase heating can be dominant. Some cases where gas phase heating was important are shown in Table IV, and the importance of cavity radius in this mechanism is shown in Figure 11. However, in the context of this model it was difficult to find cases where gas phase heating was dominant, because the available energy was usually dissipated largely in the solid phase by

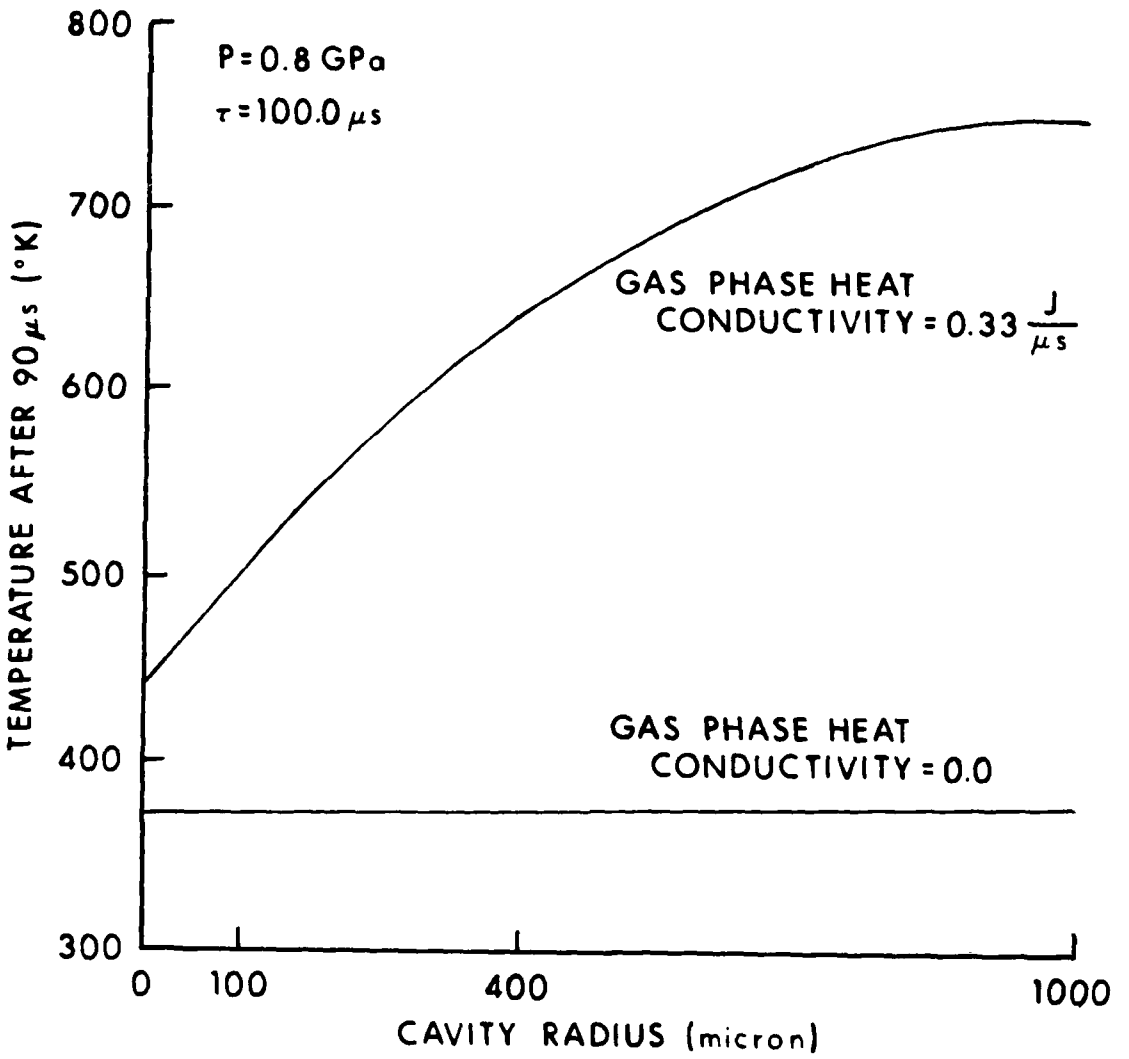

Figure 11. The maximum temperature produced in the solid due to gas phase heating is plotted as a function of cavity radius.

viscous or plastic forces. In situations where cavity collapse can occur without deformation of the solid (for instance, a planar gap at the base of an artillery shell), gas phase heating will be much more important. Starkenberg has shown that a pressure of 0.15 GPa applied to a planar gap of 0.5 mm can cause ignition in composition B.

TABLE IV: CALCULATIONS WHERE GAS PHASE HEATING WAS IMPORTANT.

Cavity Radius (micron)	Rise Time (μs)	Viscosity (Poise)	Yield Strength (GPa)	Pressure (GPa)	Gas Phase Heat Conductivity $\frac{10^3 \text{ joule}}{\text{m}^\circ\text{C}}$	Max. Temp. ($^\circ$K)
1000	100	1000	0.07	0.4	0	687
1000	100	1000	0.07	0.4	33	898*
1000	100	1000	0.7	0.4	0	463
1000	100	1000	0.7	0.4	33	635*
400	100	1000	0.7	0.4	0	361
400	100	1000	0.7	0.4	33	505*
400	100	**	0.7	0.8	0	375
400	100	**	0.7	0.8	33	656*

* Temperature was still rising when calculation was stopped.
** Calculations used the variable viscosity model described earlier.

VII. CONCLUSIONS

High temperatures may be produced in the vicinity of a collapsing cavity by viscoplastic work, plastic work, hydrodynamic compression, or gas phase heating. We have presented an analysis of the conditions where each mechanism will occur. Viscoplastic work is by far the most efficient mechanism for producing high temperatures, and it is favored by high viscosity, low yield strength, and short rise times. Using best guess estimates of viscosity (1000 poise) and yield strength (0.035 GPa), and considering pressures in the range of 0.1 to 2.0 GPa, viscoplastic work will dominate when the rise time is less than 5 to 20 microseconds. The hydrodynamic mechanism occurs when the parameters N_1 and N_2, discussed earlier, are both greater than one. This mechanism is probably never required, because other effects (viscoplastic heating) occur at the same time. For a 100 micron cavity, and using best guess estimates of yield strength and viscosity, the hydrodynamic mechanism will occur when the pressure is greater than 0.4 GPa and when the rise time (for a 0.4 GPa pulse) is less than about 8 microseconds. Smaller cavities require shorter rise times and higher pressure. Inviscid plastic work (as distinct from viscoplastic work) can cause ignition only if the melt point is higher than the ignition temperature. Gas phase heating is generally not a

dominant effect in the context of this model, because the available energy is dissipated by viscous or plastic forces rather than in the gas phase. It can be important for large cavities and relatively long rise times (which suppresses other mechanisms). If cavity closure can occur without deformation of the solid (as in a planar gap), the gas phase mechanism will be more important.

In the context of this model, cavity size and pressurization rate both have a strong effect on the temperature which may be achieved. Risetimes as short as a few tenths of a microsecond can be significantly desensitizing in some situations.

The effect of some material properties on the temperature achieved is as follows. High strength is almost always desensitizing. High viscosity is sensitizing. A low melt point can be either sensitizing or desensitizing depending on conditions, but for small cavities (a few microns) it is significantly desensitizing. Heat conductivity is important only for very small cavities (less than a micron) or for situations where gas phase heating is important. These conclusions apply only for the cavity collapse mechanism and may not be extrapolated to other situations.

REFERENCES

1. C. Mader, "Initiation of Detonation by the Interaction of Shock with Density Discontinuities," The Physics of Fluids, Vol 8, No. 10 (1965).

2. F. P. Bowden and A. D. Yoffe, Initiation and Growth of Explosion in Liquids and Solids, Cambridge University Press (1952).

3. M. C. Chick, "The Effect of Interstitial Gas on the Shock Sensitivity of How Density Explosive Compacts," Fourth Symposium on Detonation, Office of Naval Research, ACR-126 (1965).

4. G. E. Seay and L. B. Seely, Journal of Applied Physics 32, 1092 (1961).

5. J. Starkenberg, "Ignition of Solid High Explosive by Compression of an Adjacent Gas Layer," Seventh Symposium (International) on Detonation, Naval Surface Weapons Center, NSWC MP 82-334, White Oak, MD (1981).

6. B. A. Khasainov, A. A. Borisov, B. S. Ermolaev, and A. I. Korotkov; "Two Phase Visco-Plastic Model of Shock Initiation of Detonation on High Density Pressed Explosives;" Seventh Symposium (International) on Detonation; Naval Surface Weapons Center, NSWCP MP 82-334 (1981).

7. M. M. Carroll and A. C. Holt, "Static and Dynamic Pore-Collapse Relations for Ductile Porous Materials," Journal of Applied Physics, Vol 43, No. 4 (1972).

8. M. M. Carroll, A. C. Holt, and B. M. Butcher; "Application of a New Theory for the Pressure Induced Collapse of Pores in Ductile Materials;" Proceedings of the International Symposium; Pore Structure and Properties of Materials, Prague (1973).

9. R. Winter and J. Field, "The Role of Localized Plastic Flow in the Impact Initiation of Explosives," Proceedings of the Royal Society of London A343 (1975).

10. R. Frey, "The Initiation of Explosives by Rapid Shear," Seventh Symposium (International) on Detonation, Naval Surface Weapons Center, NSWC MP 82-334 (1981).

11. P. Howe, R. Frey, B. Taylor, and V. Boyle; "Shock Initiation and the Critical Energy Concept;" Sixth Symposium (International) on Detonation; Office of Naval Research, ACR-211, Arlington, VA (1970).

12. R. Setchell, Combustion and Flame 43, 255 (1981).

13. M. Ben Reuven and M. Summerfield, "Theory of Bubble Dynamics in Condensed Explosives During Start-up Transient," 17th JANNAF Combustion Meeting, CPIA Publication 329, Volume II, (1980).

14. L. M. Kachanov, Foundations of the Theory of Plasticity, North Holland Publishing Company, Amsterdam (1971).

15. J. Frenkel, Kinetic Theory of Liquids, Dover Publications, New York (1955).

16. P. W. Bridgeman, The Physics of High Pressure, G. Bell and Sons, London (1949).

17. J. Wackerle, J. O. Johnson, P. M. Halleck; "Shock Initiation of High Density PETN;" Sixth Symposium (International) on Detonation; Office of Naval Research, ACR-211, Arlington, VA (1970.

18. P. M. Halleck and J. Wackerle, "Dynamic Elastic-Plastic Properties of Single Crystal Pentaerythritol Tetranitrate," Journal of Applied Physics, Volume 47, No. 3 (1976).

19. Engineering Design Handbook - Properties of Explosives of Military Interest, U.S. Army Materiel Command, Arlington, VA, AMC Pamphlet No. 706-177.

DISTRIBUTION LIST

No. of Copies	Organization
12	Administrator Defense Technical Info Center ATTN: DTIC-DDA Cameron Station Alexandria, VA 22304-6145
1	HQDA DAMA-ART-M Washington, DC 20310
1	Chairman DOD Explosives Safety Board ATTN: COL Powell Room 856-C Hoffman Bldg 1 2461 Eisenhower Avenue Alexandria, VA 22331
1	Chairman DOD Explosives Safety Board ATTN: Dr. T. Zaker Room 856-C Hoffman Bldg 1 2461 Eisenhower Avenue Alexandria, VA 22331
1	Commander US Army Materiel Command ATTN: AMCDRA-ST 5001 Eisenhower Avenue Alexandria, VA 22333-0001
1	Commander Armament R&D Center US Army AMCCOM ATTN: SMCAR-TSS Dover, NJ 07801-5001
1	Commander Armament R&D Center US Army AMCCOM ATTN: SMCAR-TDC Dover, NJ 07801-5001
6	Commander Armament R&D Center US Army AMCCOM ATTN: SMCAR-LCE Dr. N. Slagg Dr. F. Owens Mr. W. Velicky Dr. J. Pearson Technical Library Dover, NJ 07801-5001
1	Commander US Army Armament Munitions and Chemical Command ATTN: SMCAR-ESP-L Rock Island, IL 61299
1	Director Benet Weapons Laboratory US Army AMCCOM-ARDC ATTN: SMCAR-LCB-TL Watervliet, NY 12189
1	Commander US Army Aviation Research and Development Command ATTN: AMSAV-E 4300 Goodfellow Boulevard St. Louis, MO 63120
1	Director US Army Air Mobility Research and Development Laboratory Ames Research Center Moffett Field, CA 94035
1	Commander US Army Communications Electronics Command ATTN: AMSEL-ED Fort Monmouth, NJ 07703
1	Commander ERADCOM Technical Library ATTN: DELSD-L (Reports Section) Fort Monmouth, NJ 07703-5301

DISTRIBUTION LIST

No. of Copies	Organization
1	Commander MICOM Research, Development and Engineering Center ATTN: AMSMI-RD Redstone Arsenal, AL 35898
1	Director Missile and Space Intelligence Center ATTN: AIAMS-YDL Redstone Arsenal, AL 35898-5500
1	Commander US Army Missile Command ATTN: AMSME-RK, Dr. R.G. Rhoades Redstone Arsenal, AL 35898
1	Commander USA Tank Automotive Command ATTN: AMSTA-TSL Warren, MI 48397-5000
1	Director US Army TRADOC Systems Analysis Activity ATTN: ATAA-SL White Sands Missile Range NM 88002
1	Commandant US Army Infantry School ATTN: ATSH-CD-CSO-OR Fort Benning, GA 31905
1	Commander US Army Development & Employment Agency ATTN: MODE-TED-SAB Fort Lewis, WA 98433
1	Commander US Army Research Office ATTN: Chemistry Division P.O. Box 12211 Research Triangle Park, NC 27709-2211
2	Office of Naval Research ATTN: Dr. A. Faulstick, Code 23 800 N. Quincy Street Arlington, VA 22217
1	Commander Naval Sea Systems Command ATTN: Dr. R. Bowen SEA 06I Washington, DC 20362
1	Commander Naval Explosive Ordnance Disposal Technology Center ATTN: Technical Library Code 604 Indian Head, MD 20640
1	Commander Naval Research Lab ATTN: Code 6100 Washington, DC 20375
1	Commander Naval Surface Weapons Center ATTN: Code G13 Dahlgren, VA 22448-5000
1	Commander Naval Surface Weapons Center ATTN: Mr. L. Roslund, R10C Silver Spring, MD 20902-5000
1	Commander Naval Surface Weapons Center ATTN: Mr. M. Stosz, R10B Silver Spring, MD 20902-5000
1	Commander Naval Surface Weapons Center ATTN: Code X211, Lib Silver Spring, MD 20902-5000
1	Commander Naval Surface Weapons Center ATTN: R.R. Bernecker, R13 Silver Spring, MD 20902-5000
1	Commander Naval Surface Weapons Center ATTN: J.W. Forbes, R13 Silver Spring, MD 20902-5000

DISTRIBUTION LIST

No. of Copies	Organization
1	Commander Naval Surface Weapons Center ATTN: S.J. Jacobs, R10 Silver Spring, MD 20902-5000
4	Commander Naval Surface Weapons Center ATTN: J. Short, R12 Dr. C. Dickinson Dr. Kibong Kim Dr. Harold Sandusky Dr. M. Kipp Dr. P. Taylor Dr. R. Setchell Silver Spring, MD 20902-5000
1	Commander Naval Weapons Center ATTN: Dr. L. Smith, Code 326 China Lake, CA 93555
1	Commander Naval Weapons Center ATTN: Dr. R. Atkins, Code 385 China Lake, CA 93555
1	Commander Naval Weapons Center ATTN: Dr. R. Reed, Jr., Code 388 China Lake, CA 93555
1	Commander Naval Weapons Center ATTN: Dr. K.J. Graham, Code 3891 China Lake, CA 93555-6001
1	Commander Naval Weapons Station NEDED ATTN: Dr. Louis Rothstein, Code 50 Yorktown, VA 23691
1	Commander Fleet Marine Force, Atlantic ATTN: G-4 (NSAP) Norfolk, VA 23511
1	Commander Air Force Rocket Propulsion Laboratory ATTN: Mr. R. Geisler, Code AFRPL MKPA Edwards AFB, CA 93523
1	Air Force Armament Laboratory ATTN: AFATL/DLODL Eglin AFB, FL 32542-5000
1	Commander Ballistic Missile Defense Advanced Technology Center ATTN: Dr. David C. Sayles P.O. Box 1500 Huntsville, AL 35807
7	Director Lawrence Livermore National Lab University of California ATTN: Dr. M. Finger Dr. K. Scribner Dr. E. Lee Dr. C. Turver Dr. W. Von Holle Dr. E. James Technical Library P.O. Box 808 Livermore, CA 94550
12	Director Los Alamos National Lab ATTN: Mr. J. Ramsey Dr. J. Allen Dr. B. Davis Dr. R. Steele Dr. J. Dienes Dr. R. Rabie Dr. N. Johnson Dr. H. Flaugh Dr. J. Johnson Dr. P. Tang Dr. C. Forest Technical Library P.O. Box 1663 Los Alamos, NM 87545

DISTRIBUTION LIST

No. of Copies	Organization
1	Director Sandia National Lab ATTN: Dr. J. Kennedy Albuquerque, NM 87115
10	Central Intelligence Agency Office of Central Reference Dissemination Branch Room GE-47 HQS Washington, D.C. 20502

Aberdeen Proving Ground

Dir, USAMSAA
ATTN: AMXSY-D
AMXSY-MP, H. Cohen
Cdr, USATECOM
ATTN: AMSTE-TO-F
Cdr, CRDC, AMCCOM,
ATTN: SMCCR-RSP-A
SMCCR-MU
SMCCR-SPS-IL

USER EVALUATION SHEET/CHANGE OF ADDRESS

This Laboratory undertakes a continuing effort to improve the quality of the reports it publishes. Your comments/answers to the items/questions below will aid us in our efforts.

1. BRL Report Number_____ Date of Report_____

2. Date Report Received_____

3. Does this report satisfy a need? (Comment on purpose, related project, or other area of interest for which the report will be used.)_____

4. How specifically, is the report being used? (Information source, design data, procedure, source of ideas, etc.)_____

5. Has the information in this report led to any quantitative savings as far as man-hours or dollars saved, operating costs avoided or efficiencies achieved, etc? If so, please elaborate._____

6. General Comments. What do you think should be changed to improve future reports? (Indicate changes to organization, technical content, format, etc.)

CURRENT ADDRESS

Name

Organization

Address

City, State, Zip

7. If indicating a Change of Address or Address Correction, please provide the New or Correct Address in Block 6 above and the Old or Incorrect address below.

OLD ADDRESS

Name

Organization

Address

City, State, Zip

(Remove this sheet along the perforation, fold as indicated, staple or tape closed, and mail.)

FOLD HERE

Director
U.S. Army Ballistic Research Laboratory
ATTN: SLCBR-DD-T
Aberdeen Proving Ground, MD 21005-5066

NO POSTAGE
NECESSARY
IF MAILED
IN THE
UNITED STATES

OFFICIAL BUSINESS
PENALTY FOR PRIVATE USE, $300

BUSINESS REPLY MAIL
FIRST CLASS PERMIT NO 12062 WASHINGTON, DC
POSTAGE WILL BE PAID BY DEPARTMENT OF THE ARMY

Director
U.S. Army Ballistic Research Laboratory
ATTN: SLCBR-DD-T
Aberdeen Proving Ground, MD 21005-9989

FOLD HERE

END

10-86

DTIC